Catalogue Creation for Space Situational Awareness with Optical Sensors

Tyler A. Hobson and I. Vaughan L. Clarkson
School of Information Technology and Electrical Engineering,
The University of Queensland

Travis Bessell, Mark Rutten* and Neil Gordon
National Security and Intelligence Division,
Defence Science and Technology Group

Nicholas Moretti
Inovor Technologies

Brittany Morreale
United States Air Force

ABSTRACT

In order to safeguard the continued use of space-based technologies, effective monitoring and tracking of man-made resident space objects (RSOs) is paramount. The diverse characteristics, behaviours and trajectories of RSOs make space surveillance a challenging application of the discipline that is tracking and surveillance. When surveillance systems are faced with non-canonical scenarios, it is common for human operators to intervene while researchers adapt and extend traditional tracking techniques in search of a solution. A complementary strategy for improving the robustness of space surveillance systems is to place greater emphasis on the anticipation of uncertainty. Namely, give the system the intelligence necessary to autonomously react to unforeseen events and to intelligently and appropriately act on tenuous information rather than discard it.

In this paper we build from our 2015 campaign and describe the progression of a low-cost intelligent space surveillance system capable of autonomously cataloguing and maintaining track of RSOs. It currently exploits robotic electro-optical sensors, high-fidelity state-estimation and propagation as well as constrained initial orbit determination (IOD) to intelligently and adaptively manage its sensors in order to maintain an accurate catalogue of RSOs. In a step towards fully autonomous cataloguing, the system has been tasked with maintaining surveillance of a portion of the geosynchronous (GEO) belt. Using a combination of survey and track-refinement modes, the system is capable of maintaining a track of known RSOs and initiating tracks on previously unknown objects. Uniquely, due to the use of high-fidelity representations of a target's state uncertainty, as few as two images of previously unknown RSOs may be used to subsequently initiate autonomous search and reacquisition. To achieve this capability, particularly within the congested environment of the GEO-belt, we use a constrained admissible region (CAR) to generate a plausible estimate of the unknown RSO's state probability density function and disambiguate measurements using a particle-based joint probability data association (JPDA) method. Additionally, the use of alternative CAR generation methods, incorporating catalogue-based priors, is explored and tested.

We also present the findings of two field trials of an experimental system that incorporates these techniques. The results demonstrate that such a system is capable of autonomously searching for an RSO that was briefly observed days prior in a GEO-survey and discriminating it from the measurements of other previously catalogued RSOs.

1. INTRODUCTION

Performing Space surveillance and satellite control is increasingly challenging due to the growing accessibility and congestion of space. Orbital debris and the possibility of collision threaten the viability of space-faring assets, national security and safety-of-flight of manned space missions [1]. The congested geosynchronous (GEO) belt requires careful surveillance due to the international importance of communications, sensing, and scientific satellites that reside in that orbital regime. Currently, several international agencies cultivate catalogues and maintain custody of tens-of-thousands of man-made resident space objects (RSOs) based on observation data from a network of surveillance sensors. Such catalogues are used to improve Space Situational Awareness (SSA) permitting the holistic prediction and planning necessary for collision prevention. However, in an environment where growing data volumes confront fiscal and operational constraints, RSOs can become lost to the tracking system resulting in uncorrelated tracks (UCTs) [1–3]. The resolution of UCTs adds increasing burden on limited operational resources. Therefore, the

effective management of sensors and resources, and the application of innovative data processing techniques becomes vital.

In 2015 the authors proposed that the occurrence of lost RSOs resulting in UCTs [1], could be reduced by utilizing constrained initial orbit determination (IOD) and intelligent sensor steering [4]. The sensor intelligence was achieved by incorporating a process known as dynamic steering [4–6]. Dynamic steering utilises real-time observation analysis and negative information to autonomously direct a steerable sensor. The 2015 campaign proved that a autonomous sensor has the ability to quickly and intelligently determine where to locate its field of view (FOV) in order to improve the likelihood of reacquiring targets.

Since 2015 several upgrades have improved the capability of the dynamically steered sensing system. An astrometry software package has improved real-time processing capability and the satellite detection algorithms have been made more robust. Additionally, the experimental system's control software has been upgraded to enable multi-target tracking and clutter rejection schemes based on joint probability data association (JPDA). Furthermore, in the most recent trials, the use of a non-uniform prior (derived from the unclassified JSpOC catalogue [7]) as the basis for the constrained admissible region (CAR) has been implemented. Building from these upgraded methodologies, a series of two field trials in 2016 have proven an enhanced catalogue development, target reacquisition and maintenance capability.

In this paper, we offer the experimental background and field trial results of a collaborative study, between Defence Science and Technology (DST) Group and the University of Queensland (UQ), concerning the application of dynamic steering to a constrained IOD in a cluttered environment. These field trials build from previous proof-of-concept simulated trials conducted in 2015 [4]. Section 2 provides a brief review of constrained IOD via dynamic steering. Experimental system set-up and software upgrades implemented since the 2015 campaign are detailed in Section 3. Section 4 provides details about the two field trials conducted in 2016. This section outlines the experimental process and results for each field trial. Finally, Section 5 provides further discussion of the trial results. This discussion also includes information about the future development trials. Ultimately, we propose the use of dynamic steering in conjunction with constrained IOD to achieve multi-target reacquisition, catalogue maintenance, and sensor management. The methods discussed and field trial results indicate a viable means of UCT resolution and resident space object (RSO) cataloging to enhance future space surveillance systems.

2. A REVIEW OF CONSTRAINED IOD VIA DYNAMIC STEERING

The technique known as dynamic steering has recently been presented and demonstrated by the authors from UQ [4–6]. Dynamic steering uses an iterative process which exploits negative information in near real time to improve the utility of a space surveillance network's steerable sensors. Dynamic steering permits a relaxation of the traditional constraints imposed upon the collation of targeting information — particularly concerning the level of uncertainty — for cueing conventional surveillance sensors [4, 6]. So long as the target's state error distribution can be represented in high-fidelity by a sensor controller, an autonomous reacquisition can be attempted. We consequently believe that the application of this capability to problems such as reacquiring UCTs using as few as one or two images warrants investigation. Our approach presumes that sensor-RSO relative angles and angle-rates are the only measurements that may be obtained from the available imagery. Thus, we are unable to describe the requisite [8] six-dimensional state error distribution necessary for IOD, due to a lack of information pertaining to range and range-rate. Rather than measure, we infer the missing information by constraining the possible values using a uniform distribution that is bounded by an appropriate CAR (constrained admissible region). Constraints for formulating an appropriate CAR may come from an assumed orbital profile. For example, a presumed near-GEO UCT would warrant the generation of a CAR using constraints that describe a near-GEO orbit.

The sensor measurement model $p(z|z_0)$ is assumed known at time $k = 0$, where z_0 is a vector containing, for example, noisy measurements of topocentric right ascension, α_{T}, topocentric declination, δ_{T}, and their rates, $\dot{\alpha}_{\mathrm{T}}$ & $\dot{\delta}_{\mathrm{T}}$. To obtain an appropriate CAR, for inferring a distribution of range, ρ, and range-rate, $\dot{\rho}$, a method proposed by DeMars et al. [8, 9] is employed. The method bounds the possible range and range-rate parameters according to constraints to an object's feasible position, $\mathbf{r}$, and velocity, $\dot{\mathbf{r}}$. These constraints are formulated in terms of an object's specific mechanical energy, $\mathcal{E}$, described by

$$\mathcal{E} = \frac{\|\dot{\mathbf{r}}\|^2}{2} - \frac{\mu_\oplus}{\|\mathbf{r}\|} \tag{1}$$

and eccentricity, e, described by

$$e = \sqrt{1 + \frac{2\mathcal{E}\|\mathbf{h}\|^2}{\mu_\oplus^2}} \tag{2}$$

where $\mu_\oplus$ is the Earth's gravitational parameter and $\mathbf{h} = \mathbf{r} \times \dot{\mathbf{r}}$ is the object's specific angular momentum vector. These equations can be rearranged to form a relationship between range and range-rate, provided constraints to an

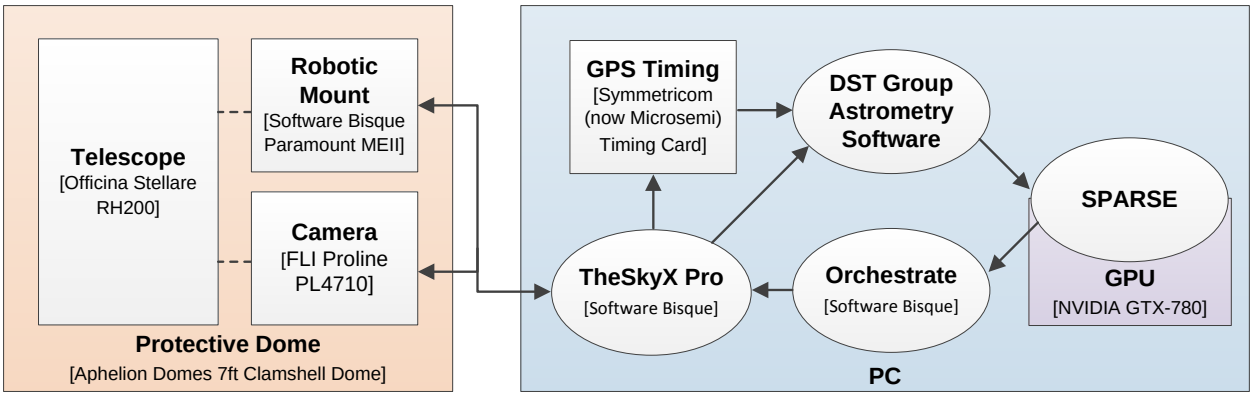

Figure 1: System architecture of the experimental system.

orbit's semi-major axis length, a [8], and eccentricity [9]. The specifics regarding the sensor-RSO geometry necessary for generating the CAR are discussed further in [9].

The density $p(z|z_0)$ and an assumed uniform distribution across the CAR may thereafter be combined to describe the six-dimensional distribution $p(z|z_0, a_1 < a < a_2, e_1 < e < e_2)$, based on the constraints $a_1 < a < a_2$ and $e_1 < e < e_2$. The distribution $p(z|z_0, a_1 < a < a_2, e_1 < e < e_2)$ can be subsequently transformed via an appropriate measurement model, $x = \mathtt{h}(z)$, to obtain the desired prior $p(x|z_0, a_1 < a < a_2, e_1 < e < e_2)$. The four-dimensional z_0 density vector is initially sampled. The resulting angles and their rates, in addition to the assumed constraints to e and a, are used to generate a CAR that is uniformly sampled to obtain range and range rate. The samples are subsequently transformed via an appropriate measurement model, $x = \mathtt{h}(z)$, to obtain a representation of the six-dimensional prior $p(x|z_0, a_1 < a < a_2, e_1 < e < e_2)$.

3. THE EXPERIMENTAL SYSTEM

DST Group is currently developing a research facility for collaborative Space Situational Awareness (SSA) experimentation. A robotic electro-optical sensor belonging to this facility, located in Edinburgh, South Australia, has been augmented with a dynamic steering capability in a collaborative effort between DST Group and UQ. The system architecture of the experimental sensor is displayed in Fig. 1. The system is composed of two primary elements, a dome to mount and house the electro-optical equipment and a PC to control the robotic telescope and implement dynamic steering.

The dome, a 7 ft Aphelion Domes clamshell, houses three crucial pieces of hardware. An Officina Stellare RH200 telescope is mounted atop a Software Bisque Paramount MEII robotic-mount, and attached to the telescope is an FLI Proline PL4710 camera. The PC, located outside of the dome, is used to operate the camera and robotic mount. These devices are commanded using a program made by Software Bisque, called TheSkyX Pro. While TheSkyX Pro acquires imagery, precise timing information is recorded from a Symmetricom (now Microsemi) GPS timing card. An additional program by Software Bisque named Orchestrate, is used to schedule and initiate multiple observations via TheSkyX Pro. Combined, these COTS elements are capable of autonomously targeting a list of predefined targets and recording time-stamped imagery returned by the sensor. It is the addition of an NVIDIA GTX-780 graphics card, DST Group's in-house astrometry software and a program named Space Particle Search Evaluation (SPARSE) [4] that provide the processing power and feedback-control necessary to implement dynamic steering.

3.1 Astrometry Software

DST Group's astrometry software correlates star catalogues with stars that have been captured in the imagery taken by the electro-optical sensor. The software can map each of the image's pixels to a specific right-ascension and declination, to within a four arc second standard deviation. Object detection is thereafter implemented in one of two ways. The software can process sidereal-stare imagery, in which the stars appear to be points and objects streak relative to a starfield background, as seen in the image on the left of Fig. 2. Alternatively, a rate-tracking method may be used to follow a target with a known trajectory and integrate its light, ideally, on a single pixel. This process causes the stars to streak and the target to appear as a bright dot – see right image of Fig. 2.

Besides accurate angular measurements, use of astrometry also offers a number of outputs that are key to achieving effective observation evaluation for dynamic steering. Notably, the software returns information about the number of

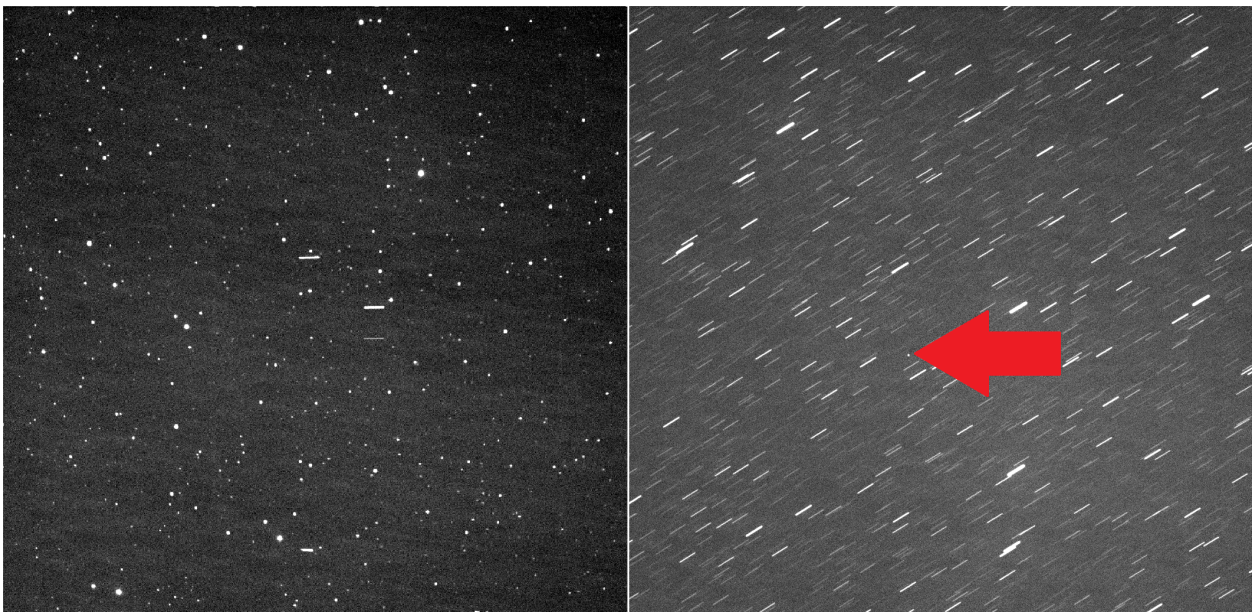

Figure 2: Left image, GEO survey sidereal tracking involving Optus C1, Optus D3, and two unanticipated objects (appearing as four streaks). Right image, example of rate tracking captured by the DST Group sensor of an RSO outside and within the FOV. The RSO appears as a single dot (indicated by the arrow) and the stars appear as streaks.

objects in the FOV, a qualitative assessment of occlusion by weather and the precise boresight angles of the sensor. Combined, these metrics are the experimental system's observation performance parameters, that are used to perform dynamic steering of the sensor as observations are processed in real-time.

3.2 SPARSE

The dynamic steering technique has been practically implemented in a computer program named SPARSE [4]. The Bayesian filtering process cannot be implemented in closed form, except in some special cases [10] that do not befit our application. In place of a pure Bayesian formulation, SPARSE implements dynamic steering via the use of a regularised particle filter (RPF) [4]. To accomplish the level of computation required for processing the filter's particle-based representation of the state error distribution, SPARSE utilises a Graphics Processing Unit (GPU) on the experimental system's graphics card [11] to efficiently compute independent processes in parallel.

To enable SPARSE to monitor and control the sensor throughout the dynamic steering process, it employs a range of physical models including planetary motion, planetary orientation, lunar motion, solar illumination, orbit propagation and sensor operation. These models enable SPARSE to monitor observability constraints, propagate the RPF's particles and anticipate the sensor's ability to detect an object at various pointing angles.

As the primary control software, SPARSE initiates observations by sending commands to the sensor via the camera and mount-control software to initiate rate-tracking observations. The resulting imagery is processed immediately by the DST Group astrometry software. Once evaluated, the observation and performance parameters are passed on to SPARSE to update the distribution and, if required, start the process over again.

4. SYSTEM TRIALS

Prior to commencing field trials, simulated trials were conducted to investigate the effectiveness of the proposed process as increasingly old imagery is used and was detailed in the authors' prior publication [4]. The simulated trial proved the viability of the proposed IOD method and assessed the probability of reacquisition of targets with the passage of time. This maiden attempt indicated the need for further refinement of the uniform sampling of the CAR taking into consideration the likelihood of range and range-rates across the CAR. It also indicated that the use of a uniform sampling of the CAR could result in large uncertainty - especially for extended periods between measurement and reacquisition. The use of a non-uniform prior was consequently a point of investigation during our subsequent field trials.

System trials were conducted in two separate field trials. The first trial involved an end-to-end field trial of the experimental system under controlled conditions. Manual data association was performed between the track and observation for this first experiment. The second field trial relaxed these conditions by extending the experimental technique to incorporate multi-target detection and probabilistic data association. The second trial also explored non-uniform sampling of the CAR via the use of a catalogue-based prior.

4.1 Field Trial 1

The first field trial involved an end-to-end trial of the experimental system while using the proposed technique under controlled conditions. When practically testing the system using non-simulated imagery, it is possible to detect other RSOs in addition to the desired target. The system can also suffer from false detections and obfuscation of the target - for instance, due to cloud. For our first field trial, we wanted to firstly ascertain if the system would work under ideal conditions. Therefore, in order to appraise the system's ability to reacquire IOD targets without these practical complications influencing the result, we attempted to isolate these influences from the experimental process by supplying a 'truth TLE' to DST Group's astrometry software. Presuming the supplied TLE is sufficiently accurate, the astrometry software is capable of determining if the target is in the sensor's FOV or not. By using this feature, any measurements made by the system could be invalidated if it could not ensure that $p_{\mathrm{D}} \approx 1$ and $p_{\mathrm{FA}} \approx 0$.

4.1.1 Field Trial 1: Experimental Process

To obtain imagery for the field trial, on the 29 February 2016 the experimental system was used to conduct a GEO-scan. The GEO-scan involved taking five images of each cell of a five-by-five grid (125 images in total) centred on the GEO-belt. Fig. 3 displays an example set of detections obtained from five images when the sensor was directed toward 55° right ascension and 5.5° declination. The FOV of the Trial 1 & 2 sensor was 2.64°, however the grid was designed so that adjacent images overlapped by approximately a quarter of the FOV. Using the GEO-scan detections, a number of RSOs could be positively correlated with the TLE catalogue and a number of suitable measurements obtained.

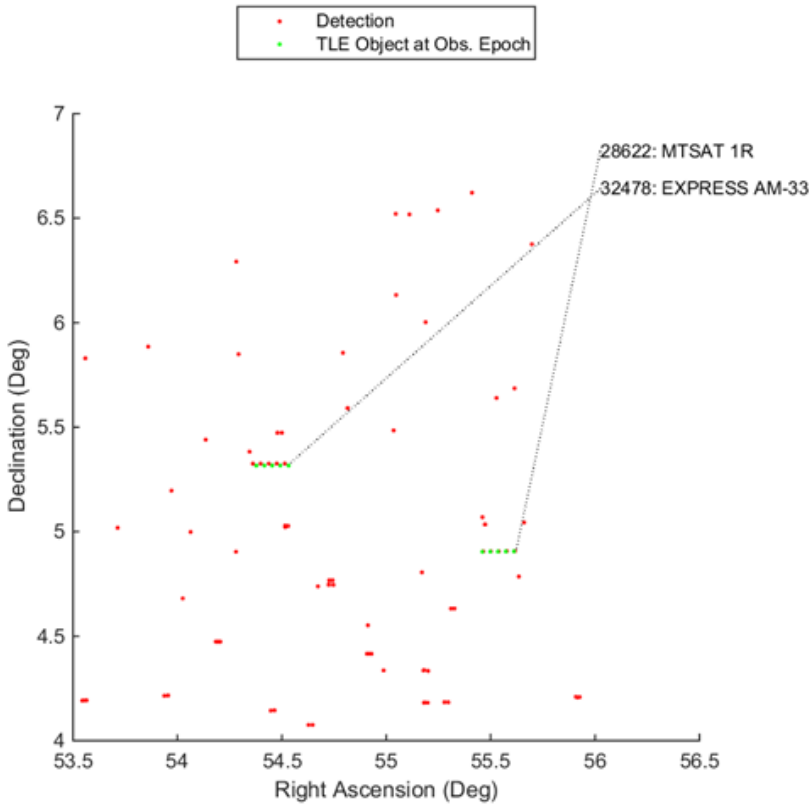

Figure 3: A sample of the GEO-scan detections — obtained 29 Feb 2016 — containing MTSAT 1R measurements and TLE correlation.

Field trials of constrained-IOD were attempted on the 2 and 3 March 2016. MTSAT 1R — US Catalogue ID: 28622 — was chosen as the test target. The first two measurements of MTSAT 1R, as shown in Fig. 3 (ordered left to right), were used to perform constrained-IOD. These measurements are detailed in Table 1.

Table 1: Measurements of MTSAT 1R's right ascension and declination on 29 February 2016.

Epoch of Measurement (UTC)	Right Ascension (Deg)	Declination (Deg)
29/2/2016 10:58:36.88	55.464	4.905
29/2/2016 10:58:46.12	55.501	4.906

The first of the two measurements was used as the observation epoch and to specify the site-relative topocentric angular position of the satellite. Both measurements were subsequently combined via the Two-point Differencing method [12] to obtain the topocentric angular velocity such that

$$z_0 \approx \begin{bmatrix} \alpha_{\mathrm{T}_1} \\ \delta_{\mathrm{T}_1} \\ \frac{(\alpha_{\mathrm{T}_2} - \alpha_{\mathrm{T}_1})}{\Delta t} \\ \frac{(\delta_{\mathrm{T}_2} - \delta_{\mathrm{T}_1})}{\Delta t} \end{bmatrix} \tag{3}$$

where α_{T} and δ_{T} are the topocentric right ascension and declination respectively, the subscript index denotes an association with either the first or second measurement in Table 1 and Δt is the time between the epoch of each measurement. In this case, $\Delta t = 9.24$s. The measurement noise model is assumed Gaussian and its covariance matrix $\mathbf{R}$ is obtained via

$$\mathbf{R} = \begin{bmatrix} 1 & \frac{1}{\Delta t} \\ \frac{1}{\Delta t} & \frac{2}{\Delta t^2} \end{bmatrix} \otimes \begin{bmatrix} \sigma^2 & 0 \\ 0 & \sigma^2 \end{bmatrix} \tag{4}$$

where $\otimes$ is the Kronecker product. As a result of a number of calibration experiments the standard deviation of right ascension and declination measurements were set to 4 arc seconds for all field trials.

Table 2 details the constraints used during the first field trial. Otherwise, all other processes were identical to the methodology used in the 2015 simulated campaign [4].

Table 2: Constraints used to define a GEO-like CAR for Campaign 2.

Parameter	Constraint
semi-major axis length	$39640583 < a < 45314809$ m
eccentricity	$0 < e < 0.05$

4.1.2 Results of Field Trial 1

In spite of sporadic cloud cover, the field trials were successfully conducted and the results are detailed in Figs. 4 – 5. Figure 4 displays the constrained-IOD reacquisition attempted on 2 March 2016. Approximately 48 hours after two images of MTSAT 1R were obtained, the experimental system employed the proposed technique involving constrained-IOD via dynamic steering and successfully reacquired the target using three observations. Figure 5 shows the features identified by the astrometry software and the successful reacquisition of MTSAT 1R on 2 March 2016 (left). Notably, the left image of Fig. 5 shows some of the cloud with which DST Group's astrometry software was confronted while attempting to make detections.

A day later, the system was reset — as opposed to continuing tracking — to see how successfully the experimental system could reacquire the target after an additional 24 hour period had elapsed. On 3 March 2016, now 72 hours after two images of MTSAT 1R were obtained, MTSAT 1R was successfully reacquired after five observations. The identification of the feature associated with MTSAT 1R is seen on the right side of Fig. 5. As anticipated from the simulated findings of our previous paper [4], MTSAT 1R took a greater number of observations to achieve reacquisition due to the increased period of time between initial measurement and reacquisition.

Field Trial 1 was successful in demonstrating that dynamic steering can be applied to reacquire objects using a fusion of sensor measurements and predefined orbital constraints. However, this trial was conducted under ideal conditions as the availability of truth information enabled the system to assume $p_{\mathrm{D}} = 1$ and $p_{\mathrm{FA}} = 0$. In order to

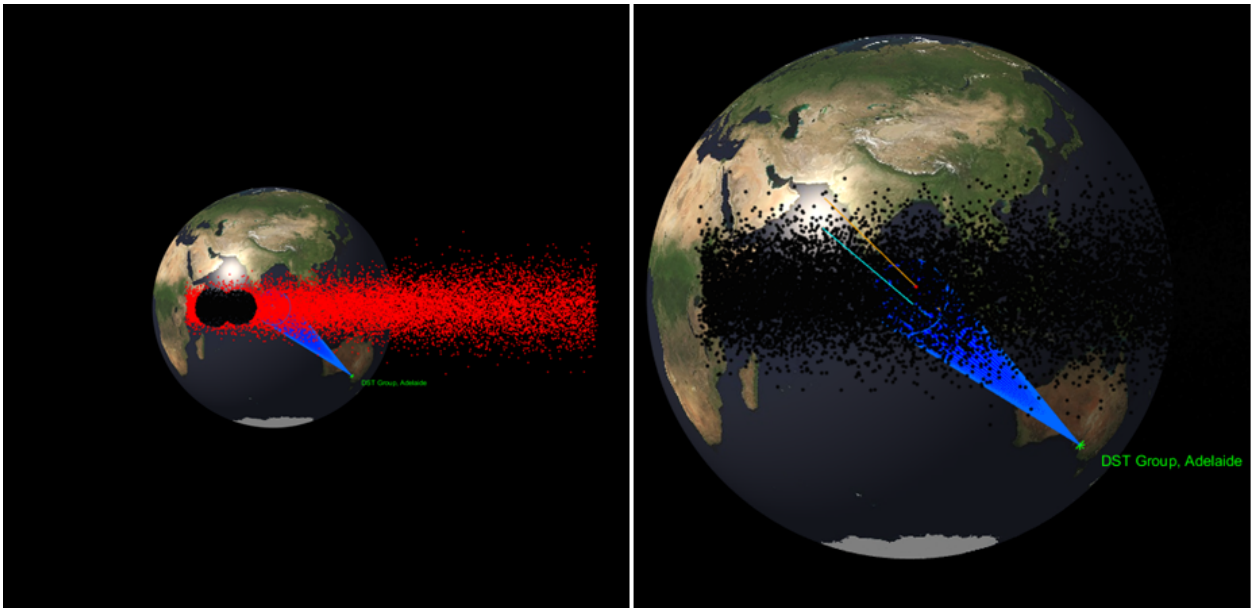

Figure 4: Images from SPARSE's particle visualisation of the observations before and after reacquiring MTSAT 1R on 2 March 2016.

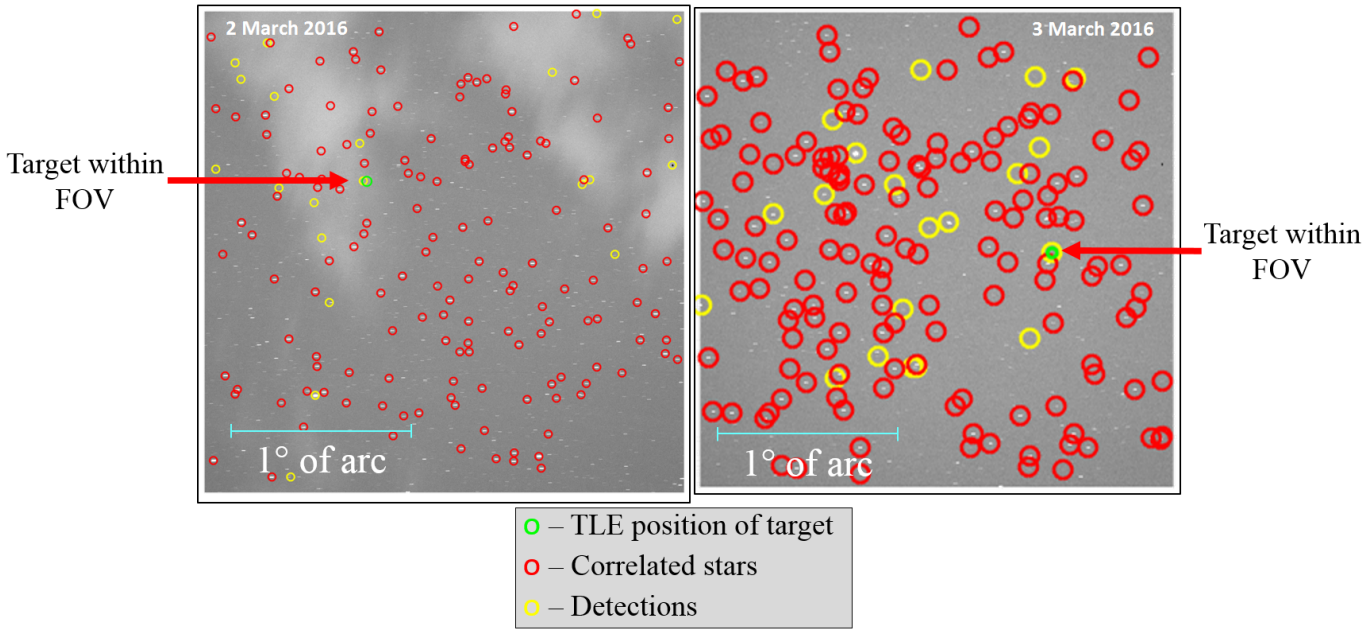

Figure 5: A visualisation produced by DST Group's astrometry software highlighting the features it has identified during MTSAT 1R's reacquisition on 2 March 2016 (left) and 3 March 2016 (right).

make the process more practical, the next objective was to expand the system in order to perform constrained-IOD under more practical conditions, such as in the presence of clutter and when detecting multiple RSOs.

4.2 Field Trial 2

The focus of the second field trial was to incorporate multi-target tracking and clutter rejection. Consequently, SPARSE was modified prior to the field trial to incorporate these two new features. Furthermore, an investigation concerning non-uniform sampling of the CAR was also conducted. The goal was to determine if a catalogue-based prior concerning the orbital constraints could be used to more effectively sample the CAR. Due to challenging meteorological conditions the trial was conducted in two parts - the first part in May and the second in August.

4.2.1 Field Trial 2: Multi-object Data Association

A joint probability data association (JPDA) method was chosen for enabling SPARSE to discriminate between detections of previously catalogued RSOs and the IOD-target. If SPARSE observes an RSO, it uses JPDA to derive a probabilistic association-weight with respect to each detection and its internal catalogue of RSOs. SPARSE thereafter performs a weighted update to the track of catalogued RSOs based on each detection and its respective association-weight. This process allows SPARSE to determine that it has not yet found the IOD-target when it unintentionally captures other known RSOs. Additionally, it enables SPARSE to update the track of known RSOs, if it happens to observe them while searching for the IOD-target.

SPARSE's implementation of JPDA was based upon the DST Group authors' prior work using JPDA and belief propagation (BP) for improving the accuracy and computational efficiency of multi-target discrimination for IOD [13]. As this work focused on using Gaussian sums to represent orbital state estimates, the JPDA algorithm was adapted for compatibility with SPARSE's RPF. The BP component of the proposed algorithm was not adapted at this stage.

Whilst JPDA affords some ability to reject clutter, a more robust method of rejection was employed to minimise p_{FA}. To distinguish between pixels illuminated by light reflected by RSOs and randomly distributed 'hot pixels' — typically caused by thermal noise — consecutive images are obtained and compared. For this study, the detections of five consecutive images are collated and analysed to identify sets of detections that appear to demonstrate propagation across the celestial background consistent with the dynamics of RSOs. As is observed in Fig. 6, when the detections of multiple images are overlaid, detections produced by RSOs are aligned in a near-linear arc. Probable detections can also be correlated with the catalogue depending on the system's confidence in an RSO's state error estimate. This methodology is demonstrated in Fig. 6 which displays a visualisation produced by SPARSE while performing a correlation. Fig. 6 shows how three of a possible five detections have been successfully associated with the estimated position of object 27603, while a set of five detections have been associated with object 39460. SPARSE thereafter uses a minimum threshold of positive detections, such as three-of-a-possible-five, to decide if a set of detections belong to an object or should be rejected as clutter.

For this study, it was necessary to ensure that only unclassified objects were detected and their positions published. Therefore, in order to demonstrate clutter rejection while adhering to this requirement, rather than use SPARSE's internal RSO catalogue, recent unclassified TLEs were used for clutter-rejection. The use of recent TLEs is *not* a requirement of the clutter-rejection process. Furthermore, the supplied TLEs were *only* made available to SPARSE for clutter rejection. They were *not* available to improve JPDA-based data association or tracking.

4.2.2 Field Trial 2: Catalogue-based prior

A secondary objective of the second field trial was to determine if the CAR could be more effectively sampled using prior information obtained from a large catalogue of RSOs. The previous trial simply assumed a uniform distribution across the CAR whilst sampling a range and range rate. If, however, a large catalogue of objects is available and it is assumed that the IOD-target belongs — or exhibits similar orbital characteristics — to a particular set of RSOs, then it is proposed that a prior that is representative of this set should, in principal, offer a more effective distribution from which to sample. To achieve this objective, the constraints themselves, eccentricity and semi-major axis length, were sampled from a prior representing the distribution of near-GEO objects in the US TLE Catalogue obtained from space-track.org [7].

Figure 7 displays the semi-major axis length and eccentricity of all unclassified TLEs in GEO-like orbits during April 2016. The distribution shows a large concentration of recently launched RSOs with geosynchronous characteristics. With the exception of some recent rocket bodies and orbital transfer engines — as verified via space-track.org [7] — there is otherwise a strong correlation between the age of the RSO and the increasing divergence from a GEO-like eccentricity, $e = 0$, and semi-major axis length, $a = 42\,164$ km. Whilst an effective method for estimating and sampling this distribution is still under investigation, for this study, an eccentricity and semi-major axis length were sampled directly from the points displayed in Fig. 7. An example constrained-IOD particle distribution produced

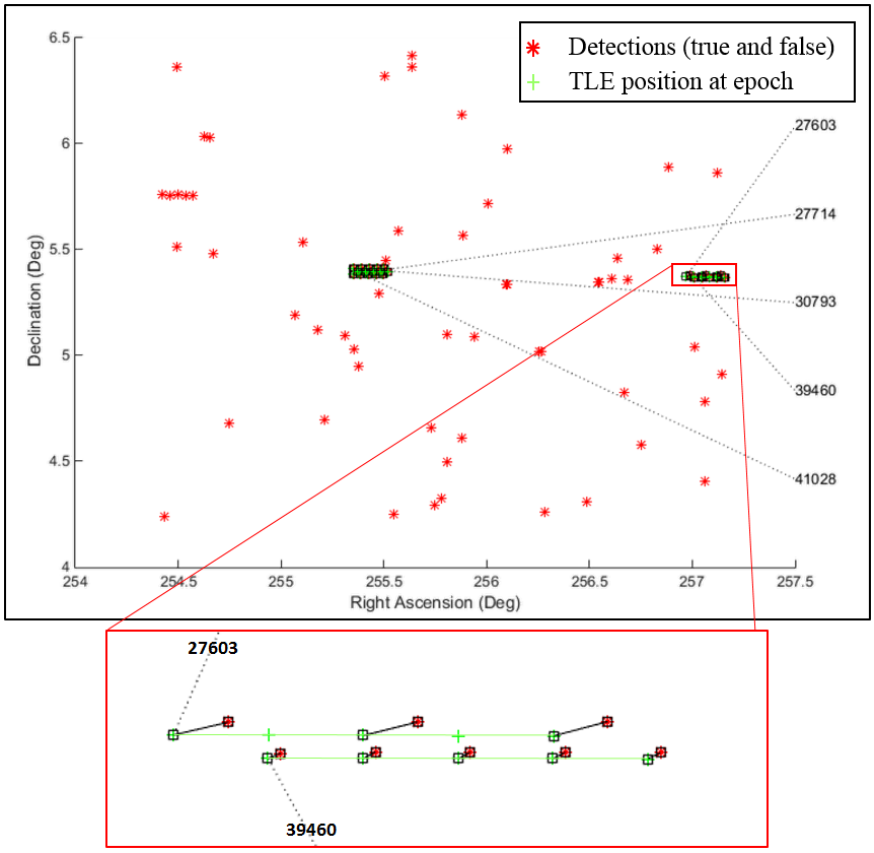

Figure 6: Visualisation produced by SPARSE's clutter rejection subroutine.

by this sampling strategy is shown in Fig. 8. In agreement with the near-GEO distribution of objects shown in Fig. 7, the particle distribution displayed in Fig. 8 has a large number of particles concentrated around the position of the original observation, with respect to the GEO-belt — representative of the large population of station-kept geosynchronous satellites — and a set of striated bands at other positions along the GEO-belt — representative of less canonical orbits of the older RSOs and modern rocket bodies/engines found in near-GEO orbits.

4.2.3 Field Trial 2: Results

The first half of field Trial 2 system-configuration was performed on 4 May 2016. This trial used measurements recorded in a GEO-scan performed 5 days earlier on 29 April 2016. During this scan, more than 20 spacecraft were observed. Observed-spacecraft's respective orbital characteristics have been highlighted in Fig. 7 via a green cross and labeled with its respective US Catalouge ID. Out of the list of visible spacecraft, GSAT 15 — US Catalogue ID: 41028 — was chosen as the first IOD-target. Its measurements were processed via the described Campaign 3 constrained-IOD methodology and the resulting distribution was loaded into SPARSE. All other visible spacecraft were also supplied to SPARSE as its catalogue of RSOs.

The first and only observation of GSAT 15 is depicted in Fig. 8. It displays SPARSE's particle visualisation shortly before and after the first reacquisition was attempted. As shown, GSAT 15 was successfully captured in the sensor's FOV. As depicted in Fig. 7, GSAT 15 (indexed as 41028) resides in the main lobe of operational spacecraft. Consequently, in spite of using a fusion of five-day-old angle measurements and a catalogue-based near-GEO orbital prior to describe a CAR, the resulting probability distribution was successfully used to autonomously direct a sensor toward GSAT 15 and perform a reacquisition in a single observation.

This trial demonstrates a significant decrease in the expected number of observations necessary to achieve reacquisition, when compared to the previous trial. However trivial the task may appear to a human operator, the system automatically recognised that the most likely location to reacquire a near-GEO object is in the same position it was previously imaged within the GEO-belt. This trial therefore demonstrates that when an IOD-target is suspected of belonging to a particular orbital regime, such as geosynchronous orbit, constrained-IOD may be utilised to quickly

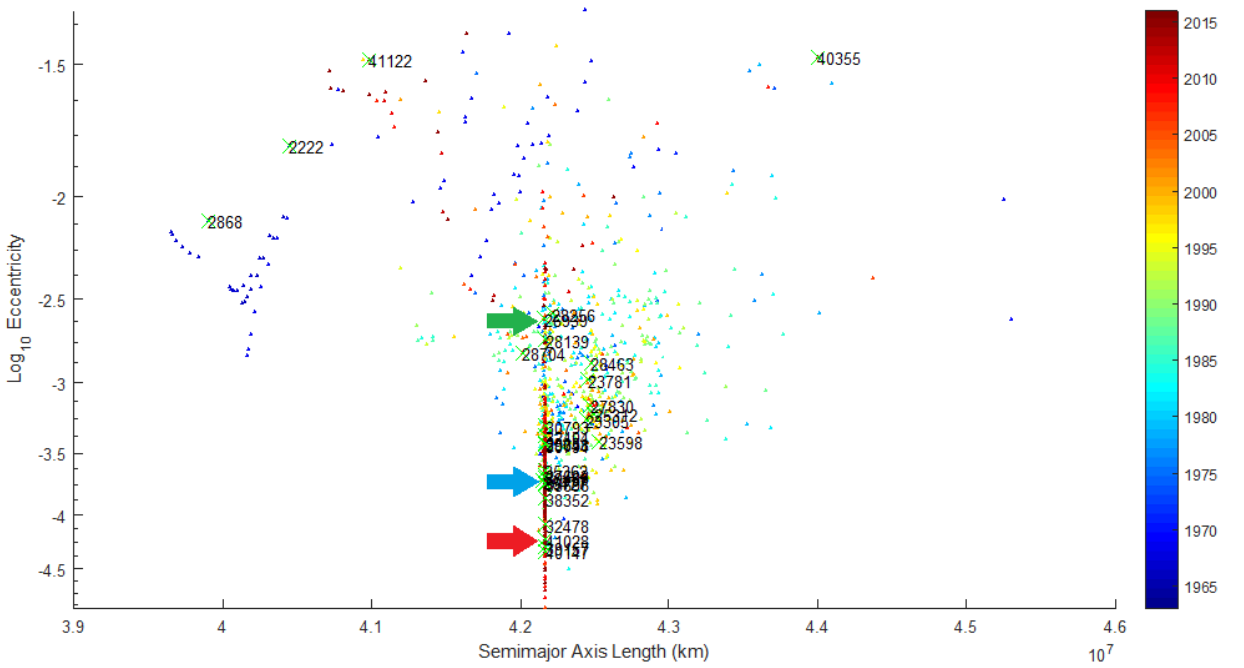

Figure 7: Distribution of near-GEO unclassified RSOs coloured according to the year in which they were launched. The three targets used during field trial two, 41028 (red arrow), 27603 (blue arrow) and 26939 (green arrow), exhibit the variation in eccentricity used to exercise the SPARSE system. Created August 2016.

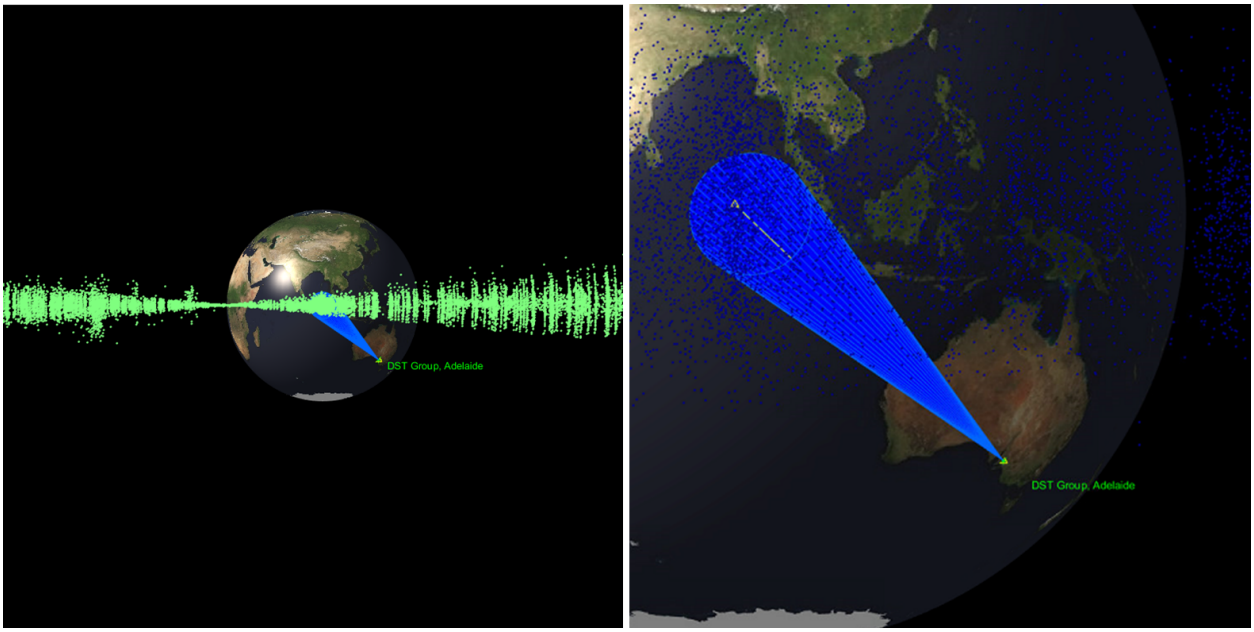

Figure 8: Images from SPARSE's particle visualisation of the observations before and after reacquiring GSAT 15 on 4 May 2016.

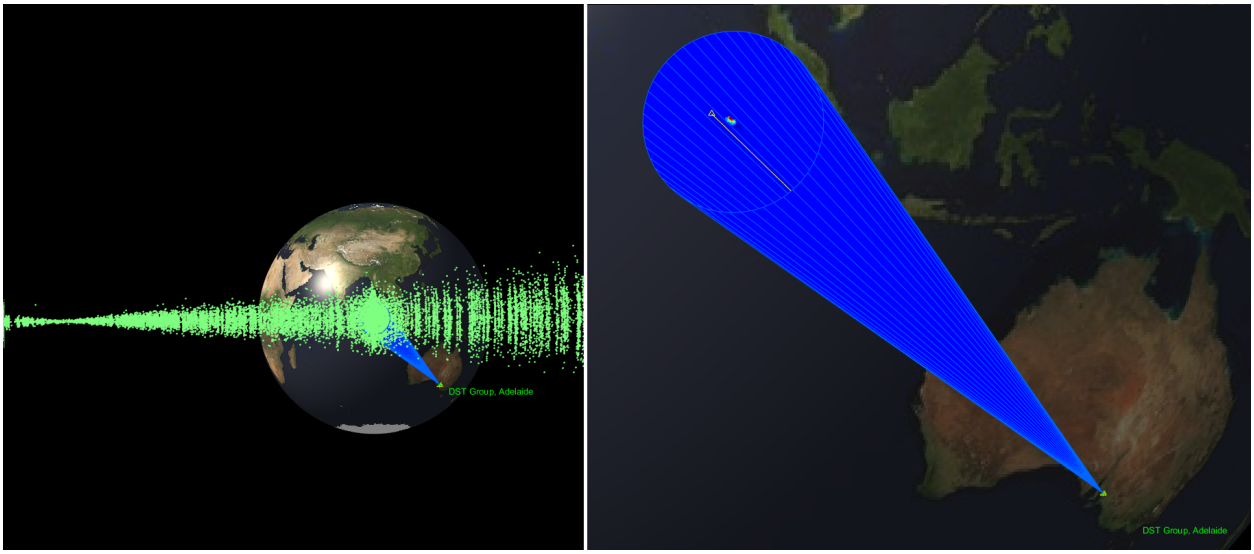

Figure 9: Images from SPARSE's particle visualisation, captured before and after SPARSE successfully reacquired NSS 6 in its FOV during it's first attempt on 26 August 2016. SPARSE correctly identified the object and began tracking and performing catalog updates.

and automatically ascertain the validity of that conjecture. But as not all near-GEO objects belong to Fig. 7's main lobe, a follow-up experiment was conducted to determine how effectively a non-canonical target could be reacquired.

Trial 2 was re-initiated in August 2016. Before conducting this follow up phase of Trial 2, it was determined that the introduction of JPDA to a particle-based implementation of dynamic steering was incompatible with SPARSE's established routines for avoiding particle degeneracy within the RPF. This meant that particle degeneracy needed to be manually prevented. Consequently, as target reacquisition was the goal, rather than tracking accuracy, for this phase we have temporarily increased the measurement model's angular standard deviation during dynamic steering. The measurement model used during CAR generation was not altered. This change to dynamic steering mitigated the degeneracy issue. However, we intend to undergo further testing to robustly approach degeneracy in SPARSE's new multi-target tracking.

Three total GEO scans were performed on 22 and 23 August resulting in the detection and TLE correlation of thirty-one unique GEO and near-GEO objects. Four days after the initial GEO scan SPARSE was used to reacquire NSS 6 (27603) and S/L 12 RB-2 (26939). SPARSE successfully reaquired object 27603 on the first attempt as seen in Fig. 9. Even with initial observations that were 4 days old, SPARSE consistently re-acquired targets that resided in the main GEO lobe on the first attempt.

Nevertheless, to further exercise SPARSE, S/L 12 RB-2 (26939) was chosen as a more challenging case due to variation in eccentricity from the main lobe of GEO RSOs. As seen in Fig. 7, S/L 12 RB-2 resides in a slightly higher orbit than most GEO-RSOs and its eccentricity is larger than most RSOs belonging to the main lobe. Even with this more challenging case, SPARSE reacquired the target on the first attempt and successfully correlated the detection with the IOD generated on Monday 22 August as seen in Fig. 10.

5. DISCUSSION

The results of the two field trials conducted demonstrate that dynamic steering can be applied to reacquire objects using a fusion of measurements and orbital constraints. But in order to become a practical tool for operational use, the system must operate in the presence of noise and detections of other objects. The JPDA-based data-association and contiguous imaging used in the second field trial were successful at achieving these goals but refinement or replacement of the proposed strategies are required for increased utility and robustness of the constrained-IOD technique.

The catalogue-based CAR sampling strategy was successful at demonstrating that sampling uniformly from the CAR may be a significantly inferior approach if more than just the bounds are known about an IOD-target's orbital constraints. The refinement of this non-uniform CAR distribution based on an RSO's expected orbital characteristics may improve maintenance of target's state estimate and search methods, offering a potential solution for UCT correlation in an increasingly cluttered environment. Further investigation into the representation and sampling of densities correlated to specific orbital characteristics of catalogued RSOs is warranted and recommended.

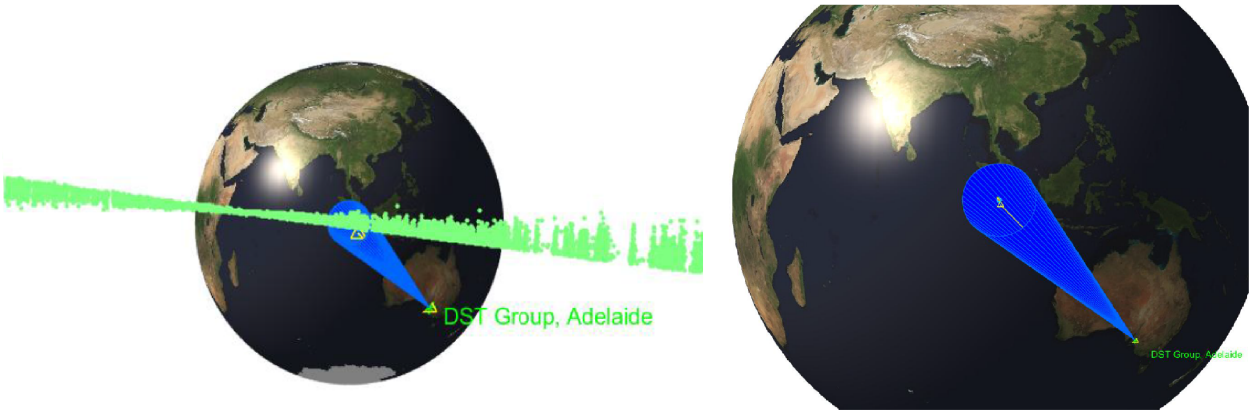

Figure 10: Images from SPARSE's particle visualisation, captured before and after SPARSE successfully reacquired S/L 12 RB-2 in its FOV during it's first attempt on 26 August 2016. SPARSE correctly identified the object and began tracking and performing catalog updates.

Furthermore, the use of alternate sampling methods, such as Markov chain Monte Carlo (MCMC) [14], will be explored in upcoming experimental campaigns. Additionally, continued experimentation will be performed to refine our approach to particle degeneracy in order to approach the minimum state error uncertainty afforded by our sensor. Future upgrades include the expansion of CAR sampling methodologies to include IOD and reacquisition of targets in other orbital regimes, such as LEO.

The field trials were heavily impeded due to cloud. Whilst favourable weather and sensor-site selection play a role, continued investigation of dynamic steering would benefit greatly from the development and integration of a cloud/obscuration filter into the image processing software. Ideally, this software would assign a probability of obscuration to regions within each image returned by the sensor. Using this information, a non-uniform probability of detecting a target — due to obscuration — can be applied to the section of the prior that coincides with the sensor's FOV.

The catalogue development and maintenance techniques discussed in this paper and demonstrated throughout the two trials offer a new and promising framework for catalogue maintenance and sensor management. In an environment of increasingly limited resources and accelerating demands, the effective prioritization of tasks for space surveillance network assets is critical. Using autonomous sensors to swiftly reacquire targets based on one or two images, even after long periods without observations, provides a key capability for future space surveillance systems.

REFERENCES

[1] National Research Council of the National Academies, *Continuing Kepler's Quest: Assessing Air Force Space Command's Astrodynamics Standards*. The National Academies Press, 2012.

[2] M. Wasson, "Space situational awareness in the Joint Space Operations Center," in *Air Force Air and Space Operations Center (614th) Peterson AFB Co.*, 2011.

[3] T. Kelecy and M. Jah, "Analysis of orbit prediction sensitivity to thermal emissions acceleration modeling for high area-to-mass ratio (HAMR) objects," in *Proc. the Advanced Maui Optical and Space Surveillance Technologies Conf., (AMOS)*, 2009.

[4] T. A. Hobson, C. Gordon, Neil, I. V. L., M. Rutten, and T. Bessel, "Dynamic steering for improved sensor autonomy and catalogue maintenance," in *Proc. the Advanced Maui Optical and Space Surveillance Technologies Conf., (AMOS)*, 2015.

[5] T. A. Hobson and I. V. L. Clarkson, "A Particle-based Search Strategy for Improved Space Situational Awareness," 3-6 Nov 2013, accepted in Asilomar Conf. on Signals Systems, and Computers.

[6] ——, "An experimental implementation of a particle-based dynamic sensor steering method for tracking and searching for space objects," 4-9 May 2014, accepted in proceedings of IEEE International Conference on Acoustics, Speech and Signal Processing (ICASSP).

[7] USSTRATCOM, "Space Track," 2004, [Online]. Available: www.space-track.org.

[8] K. J. DeMars, M. K. Jah, and P. W. Schumacher Jr, "Initial orbit determination using short-arc angle and angle rate data," *Aerospace and Electronic Systems, IEEE Transactions on*, vol. 48, no. 3, pp. 2628–2637, 2012.

[9] K. J. DeMars and M. K. Jah, "Probabilistic initial orbit determination using gaussian mixture models," *Journal of Guidance, Control, and Dynamics*, vol. 36, no. 5, pp. 1324–1335, 2013.

[10] B. Ristic, S. Arulampalam, and N. Gordon, *Beyond the Kalman Filter*. Artech House, 2004.

[11] T. A. Hobson and I. V. L. Clarkson, "GPU-based space situational awareness simulation utilising parallelism for enhanced multi-sensor management," in *Proc. the Advanced Maui Optical and Space Surveillance Technologies Conf., (AMOS)*, 2012.

[12] Y. Bar-Shalom, X. R. Li, and T. Kirubarajan, *Estimation with applications to tracking and navigation: theory algorithms and software*. John Wiley & Sons, 2004.

[13] M. Rutten, J. Willams, N. Gordon, J. Stauch, J. Baldwin, and M. Jah, "A comparison of JPDA and belief propagation for data association in SSA," in *Proc. the Advanced Maui Optical and Space Surveillance Technologies Conf., (AMOS)*, 2014.

[14] D. Gamerman and H. F. Lopes, *Markov chain Monte Carlo: stochastic simulation for Bayesian inference*. CRC Press, 2006.